Lab on a Chip

Accepted Manuscript

ROYAL SOCIETY OF CHEMISTRY

www.rsc.org/loc

Journal Name

RSCPublishing

ARTICLE

Wide bandwidth power amplifier for frequency-selective insulator-based dielectrophoresis

Cite this: DOI: 10.1039/x0xx00000x

Vahid Farmehini[a], Ali Rohani[a], Yi-Hsuan Su[a] and Nathan S. Swami[a,*]

Received 00th January 2012,
Accepted 00th January 2012

DOI: 10.1039/x0xx00000x

www.rsc.org/

Insulator-based dielectrophoresis enables contact-less separation and analysis of biosystems, but it is unable to operate effectively in the MHz frequency range, which is necessary for the manipulation of biological cells based on the characteristic electrophysiology of their cytoplasm or biomolecular preconcentration based on their unique conformation. To address the steep drop in output power and the rise of signal distortions within conventional amplifiers at MHz frequencies due to slew rate limitations, we present the design principles for a wideband amplifier. This is validated by demonstrating the absence of harmonic distortions and parasitic DC within the amplifier output up to 15 MHz, thereby enabling analysis of cytoplasmic alterations on oocysts of *Cryptosporidium parvum*, due to constant force dispersion in the MHz range.

Introduction

Dielectrophoresis enables frequency-modulated manipulation of polarized bio-particles under a spatially non-uniform electric field[1, 2] and is widely applied towards the selective transport, separation and characterization of biosystems[3]. In particular, its application as electrode-less[4, 5] or insulator dielectrophoresis[6, 7] (iDEP), wherein the polarized particles are directed towards (by positive DEP or pDEP) or away (by negative DEP or nDEP) from spatially localized regions of high field caused by insulating constrictions in a microfluidic device, offers unique advantages for the sorting and analysis of biosystems. First, in comparison to electrode-based methods, problems associated with field-induced adhesion and destruction are reduced[8], since bio-particles are manipulated in an electrode-less or contact-less manner[9], across a wide spatial extent spanning the entire device depth, thereby enhancing throughput. Second, this design enables facile integration of DEP preconcentration of analytes with a variety of sensing paradigms, since the polarized particles are not trapped at the vicinity of the electrodes driving the DEP, but at insulator constriction regions where capture probes can be immobilized for enabling selectivity through bio-recognition strategies[10]. However, the electrodes driving the DEP field orthogonal to the fluid flow are typically spaced considerably from each other (~0.5-2 cm) to ensure a wide spatial extent for particle manipulation and to facilitate the absence of field distortion and bio-particle damage that can occur due to electrode edges within the channel. Hence, there is a need for higher voltages (typically 100-1000 V_{RMS}) than required with electrode-based DEP (typically 10-20 V_{RMS}) to ensure the necessary field for trapping particles of low polarizability, even within 3D constrictions[11] or nano-device designs that enhance localized field[12, 13]. This high voltage requirement is particularly problematic for conducting iDEP in the MHz frequency ranges, due to the performance degradation of commercial amplifiers. As a result, a majority of iDEP studies are restricted to DC fields[14], or low frequency AC fields[15] (<500 kHz), where the discrimination is based only on cell membrane integrity, rather than on the electrophysiology of cellular cytoplasm (1-10 MHz) or nucleoplasm (>40 MHz), or the unique conformation of biomolecules (>1 MHz). Herein, we describe the design principles for constructing a wideband power amplifier for performing iDEP at MHz frequencies. Based on counter-phase coupling of two operational amplifiers (Op-amps) by using a splitter to ensure 180° phase-shifted signals over a large bandwidth, in conjunction with an adjustable power supply and attenuator to arrest dissipation, we maximize the output power up to 15 MHz, while avoiding signal distortion. This is validated by demonstrating the absence of harmonic distortions and parasitic DC offset fields within the amplifier output at MHz frequencies, since all of these adversely affect DEP trapping. The application of this wideband amplifier for enabling quantitative DEP analysis of 3 μm sized *Cryptosporidium parvum* (*C. parvum*) bio-particles is demonstrated by comparing its performance to state-of-the-art commercial amplifiers currently on the market. This instrumental innovation has been essential towards achieving quantitative iDEP based separation of subpopulations of *C. parvum* oocysts based on sporozoite integrity in their cytoplasm (at 1-10 MHz)[16, 17] and towards coupling iDEP preconcentration to the detection of biomarkers (neuropeptide Y at ~3 MHz)[18]. We envision its application towards enabling distinctions based on electrophysiology of cell cytoplasm and nucleoplasm for separating stem cell subpopulations[19].

Methods: The Design Process

The literature on wideband power amplifiers is scarce. Prior work has focused on amplifying voltages (up to 1 kV) for operation at frequencies up to only a few hundred KHz,[20] rather than at higher frequencies. State-of-the-art commercial power amplifiers (FLC Elec. A400DI, Trek Inc. 2100HF and Thorlab Inc. HVA200) are able to operate up at ~500 V_{pp} until 500 kHz, after which they exhibit a steady drop in power. The design of our wideband amplifier circuit is based on high speed power operational amplifiers (Op-amps) rather than on discrete transistors, since Op-amps are highly predictable ICs, in terms of gain and signal shape, with no need for particular biasing or stabilizing components. **Fig. 1** shows the overall circuit.

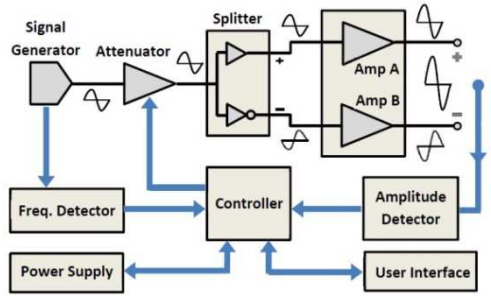

Fig 1. Block diagram for the wideband amplifier circuit.

High speed dual-amplifier and Splitter

The speed of power Op-amps under high voltage settings is limited by their slew rate. Slew rate is the maximum rate of change of output voltage per unit time (V/µs). Limitations in slew rate capability can give rise to distortions in signal shape of the amplifier output. For a sinusoidal signal, the slew rate (SR) capability at all points in an amplifier must satisfy:

$$Slew\ rate\ (SR)\ \geq\ \pi \times V_{pp} \times f \qquad (1)$$

Here, f is the signal frequency and V_{pp} is the peak-peak amplitude of the signal. Hence, to obtain a sinusoidal signal output at 5 MHz with amplitude of 250 V_{pp}, we need an Op-amp with a slew rate of: 4000 V/µs. This is far beyond the capability of any ultrafast power Op-amp in the market. PA107DP from APEX Micro, for instance, is capable of slew rates only up to 2500 V/µs. To address this limitation, we feed two identical PA107DP Op-amps with counter-phase signals of the same amplitude. In this manner, whenever the output of one Op-amp is at its maximum, the output of the other Op-amp is at its minimum, thereby causing a voltage difference between the two outputs, which is twice that of each individual output. However, the Splitter unit that synchronizes these counter-phase signals needs to be designed with super-fast low-power Op-amps (Texas Instruments LM7171) to obviate deviation from the 180° phase difference, for eliminating distortion and nonlinearity over a wide range of input signals and frequencies.

Self-adjustable Power Supply

Power dissipation (P_D) inside the Op-amps can limit the maximum output power at high frequencies. If the output current is small ($P_{Load} \ll P_D$), then for two symmetrical high-voltage supplies ($\pm V_S$) with supply current (I_S), P_D is given by:

$$P_D\ =\ \left(V_S^{+}\ -\ V_S^{-}\right) \times I_S = 2V_S I_S \qquad (2)$$

With increasing frequency, the power dissipation first rises due to the higher supply current (I_S) from the lower internal impedances, while at even higher frequencies, the dissipation eventually falls due to diminishing output gain, thereby causing a peak in power dissipation at ~5 MHz. Hence, a self-adjustable Power Supply is utilized for dynamic modulation of the supply voltages (V_S) at each working frequency, to ensure minimal dissipation in the 3-7 MHz range. In this manner, we can compensate for the drop in gain at higher frequencies by adjusting for the optimal input signal levels required to maximize output power, while avoiding over-heating and reducing signal distortion over a wide frequency range.

Attenuator and Controller unit

The Op-amp gain drops steadily at frequencies above 1 MHz. Therefore, larger input signals are required at successively higher frequencies for maximizing output amplitude. However, if this large input signal is maintained at lower frequencies then the output waveform will be distorted from sinusoidal to that resembling a square wave, which increases power dissipation and distortion due to operation in the saturation regime. Hence, based on the detected signal amplitude and frequency, a controller unit adjusts the gain using a set of reed-relay switches, while the attenuator modulates the input signal to limit the output to a constant user-defined voltage (V_{max}).

Figures of merit for signal characteristics

The performance of the wideband amplifier was compared to that of a so-called conventional amplifier (FLC A400DI), since this is the only product with an output of 300 V_{pp} up to 1 MHz. The respective amplifiers were compared based on the frequency response of their output amplitude and distortion. Based on signal shapes (Tektronix TDS3012B-NV), the parasitic DC and amplitude at each harmonic frequency (V_n) were used to compute Total Harmonic Distortion (THD):

$$THD = \frac{\sqrt{V_2^2+V_3^2+\cdots+V_n^2}}{V_1} \qquad (3)$$

DEP force quantification

Comparison of the levels of positive DEP on *Cryptosporidium parvum* in the MHz range was performed by using the respective amplifiers within an electrode-less iDEP device. Neglecting inter-particle interactions, the DEP force values were calculated using frame-by-frame tracking of the trapped particles to extract their displacement vectors (x and y) over time (t) to compute F_{DEP} using:

$$F_{DEP} = m\frac{d^2x}{dt^2} - 6\pi\eta a\frac{dx}{dt} \qquad (4)$$

Here, m and a are the mass and radius of the particles and η is the viscosity of the fluid, as per ESI and prior work[17].

Results and Discussion

Comparison of amplifiers for signal characteristics

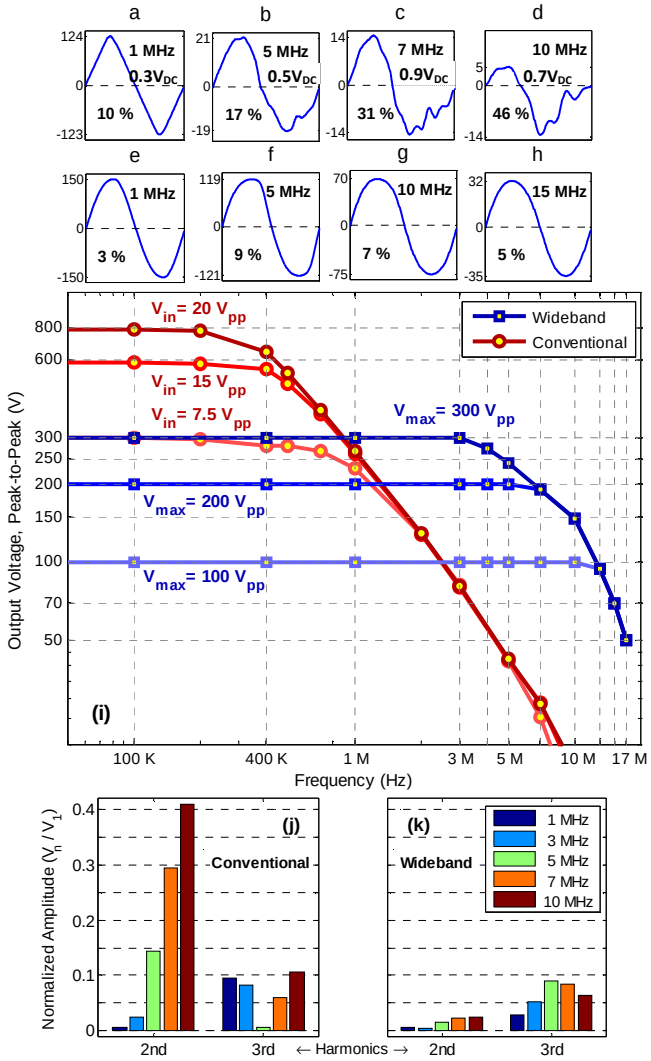

Fig 2. Output waveform of conventional amplifier (FLC A400DI) for V_{in} = 15V_{pp} (a-d) vs. wideband amplifier (e-h) in the 1-15 MHz range (DC offset and THD are indicated). (i) Frequency responses of wideband amplifier (blue) at the indicated V_{max} levels vs. the conventional amplifier (Red) at the indicated V_{in} levels. Normalized amplitudes (V_2/V_1) and (V_3/V_1) at 1-10 MHz for: (j) conventional amplifier and (k) the wideband amplifier.

The frequency responses of the output amplitude and signal distortion from the wideband amplifier are compared to those from the FLC A400DI amplifier in **Fig. 2**. It is apparent that while the conventional amplifier offers greater voltage in the low frequency range (<800 kHz), the output from the wideband amplifier is far higher, onwards from 1 MHz. Furthermore, the conventional amplifier shows a highly distorted signal shape at successively higher frequencies in the MHz range, as per **Fig. 2a-d**, whereas the sinusoidal wave-shapes are preserved in the MHz range for the wideband amplifier (**Fig. 2e-h**). The signal distortion and parasitic DC levels are quantified in **Fig. 2j-k** (Details as a table in ESI). Herein, parasitic DC levels from the conventional amplifier exhibit a steady rise with increasing frequency due to the increasing difference in DC levels at the two channels of the amplifier. While the absolute parasitic DC levels are small, they become a greater fraction of the output at higher frequencies, since slew rate limitations cause a steep decline in V_{RMS} output at the fundamental frequency. For instance, while the V_{RMS} to parasitic DC ratio is 250 at 1 MHz, it drops steeply to 28 at 5 MHz, and to just 8 at 10 MHz.

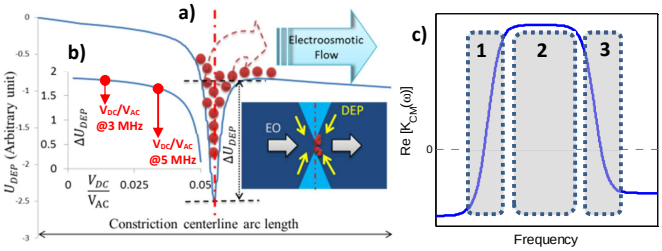

Fig 3. (a) Influence of DC offset on AC field driven pDEP, as quantified in (b). (c) Three regions of polarizability dispersion, containing the main harmonics.

This steady rise of parasitic DC in proportion to the AC field causes electrophoretic (F_{EP}) and electroosmotic (F_{EO}) forces to influence the net force balance. While these DC-driven electrokinetic forces tilt the potential profile to enhance trapping under nDEP, they also cause the leakage of particles under pDEP trapping (**Fig. 3a**). In fact as per **Fig. 3b**, beyond critical levels, the offset DC field obtained using the conventional amplifier at frequencies beyond 5 MHz can cause a significant reduction in the DEP trapping potential (ΔU_{DEP}). On the other hand, the parasitic DC levels are negligible for the wideband amplifier, thereby offering highly quantitative DEP force dispersions. An alternate problem with conventional power amplifiers is the emerging harmonic distortion at MHz frequencies. Herein, the amplitude levels of the higher order harmonics are large enough to cause a deviation of the sinusoidal wave shape, from a single frequency signal to one that includes signals at several harmonic frequencies, thereby influencing the polarizability dispersion (**Fig. 3c**). This waveform distortion arises due to phase shift deviations at high frequency from the required counter phase signal input to the Op-amps or due to the operation of Op-amps at their saturation level at low frequencies. As per the normalized amplitude at each harmonic with respect to the fundamental frequency (V_n/V_1) in **Fig. 2j-k,** significant distortions are apparent with the conventional amplifier beyond 5 MHz, especially at the second harmonic, whereas the distortions are much weaker with the wideband amplifier. While a sine wave signal has zero THD (only one harmonic), triangular and symmetrical square waves exhibit THDs of 0.12 and 0.48, respectively. The implication of this harmonic distortion is alterations in DEP force magnitude and in some scenarios, the force direction too. For instance, **Fig. 3c-2** considers the scenario wherein the fundamental frequency and the harmonics cause pDEP with relatively constant polarizability dispersion (Re(K_{CM})). We can then calculate the altered DEP force (F_{DEP}) due to the distorted signal (THD) with peak-peak amplitude of V_1 (fundamental), as a function of the ideal sinusoidal signal of peak-peak amplitude V_{pp} that causes F_{Ideal} (details in ESI):

$$F_{DEP} = (1 + THD^2)\left(\frac{V_1}{V_{pp}}\right)^2 F_{Ideal} \qquad (5)$$

Here, the frequency dependent term: $(1+THD^2)$ influences the force dispersion, due to contributions of the higher order harmonics, whereas the term: $(V_1/V_{pp})^2$, reflects the alteration in maximum amplitude of the output signal due to deviation from the ideal sinusoidal wave shape. Hence, while the distorted quasi-triangular wave shape of the conventional amplifier causes a reduction in DEP force by just 20% at 1 MHz (due to 10% THD and V_1/V_{pp}=0.9), the respective force reductions are substantial at 5, 7 and 10 MHz. On the other hand, since the THD of the wideband amplifier is less than 10% and V_1/V_{pp} remains close to unity, the DEP force alteration is less than 5% over the MHz range. Next, considering the scenario where the fundamental frequency is in the nDEP region, whereas the harmonics lie in the pDEP frequency region (**Fig. 3c-region 1**), then the force would be further distorted, since the $Re(K_{CM})$ is no longer constant but rather varies with each harmonic signal. For instance, if K_{CM} at the fundamental frequency is $K_{CM}(\omega_1)$ and that for the next significant higher order harmonic is $K_{CM}(\omega_m)$, then Eq. (5) can be modified (details in ESI):

$$F_{DEP} = (1+\alpha THD^2)\left(\frac{V_1}{V_{pp}}\right)^2 F_{Ideal};\ \alpha = \frac{Re[K_{CM}(\omega_m)]}{Re[K_{CM}(\omega_1)]} \qquad (6)$$

In the scenario wherein the fundamental frequency (ω_1) is in the nDEP region close to crossover towards pDEP, whereas the next significant harmonic (ω_m) is in the pDEP region, as in **Fig. 3c-1**, then: $\alpha \ll -1$, since K_{CM} under nDEP (ω_1) is usually less than that under pDEP (ω_m). This causes greater DEP force distortions from F_{Ideal} than the scenario in **Fig. 3c-2**. In fact, at high enough THD values, the direction of the DEP force could also be altered. A similar scenario can occur at ultra-high frequencies near the second DEP crossover region (**Fig. 3c-3**).

Comparison of amplifiers for iDEP dispersion in MHz range

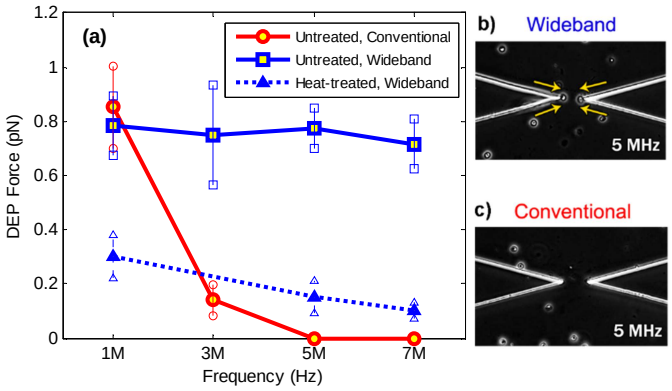

Fig 4. Measured DEP force dispersion of *C. parvum* in the 1-7 MHz region using the conventional vs. wideband amplifier (Videos in ESI).

Finally, we present a comparison of the DEP force dispersion in the MHz range on the iDEP device using the conventional versus the wideband amplifier, with oocysts of *C. parvum* as the model bio-particle. We focus on the DEP force dispersion in the 1-7 MHz range, where the polarized oocysts exhibit positive DEP due to the dominance of cytoplasm conductivity, thereby causing trapping at the constriction tip. The DEP force data in **Fig. 4** (videos in ESI) show that while the trapping under pDEP using the conventional amplifier is clear at 1 MHz, it is less clear at 3 MHz and absent at 5 MHz. On the other hand, with the wide bandwidth amplifier, trapping force on untreated oocysts is significant and at a constant level in the 1-7 MHz range. As a result, differences in force dispersion are easily apparent in the MHz range for probing the cytoplasm of untreated versus heat treated oocysts, whereas these are not apparent using the conventional amplifier.

Conclusion

To enable electrode-less or contact-less manipulation of biosystems in the MHz frequency range, we present the design principles for a wideband power amplifier to address the steep drop in amplitude and the rise of signal distortion that occurs within conventional amplifiers. Through counter-phase coupling of two operational amplifiers by using a wideband splitter circuit, in conjunction with a self-adjustable power supply and an attenuator to deliver a constant power output for avoiding over-heating and signal distortion due to saturation, we are able to achieve the necessary power up to 15 MHz. This is validated by demonstrating the reduction of harmonic distortions and parasitic DC effects within the amplifier output, as well as the ability to discern cytoplasmic alterations in oocysts of *C. parvum*, due to the constant level of pDEP force dispersion on untreated oocysts in the 1-7 MHz range.

Acknowledgements

Support from NSF 1332329 and Virginia Biosciences Health Research Corporation (VBHRC) is acknowledged.

Notes and references

[a] Department of Electrical & Computer Engineering, University of Virginia, Charlottesville, VA 22904.

Electronic Supplementary Information (ESI): details on the iDEP device, F_{DEP} computation method, proof of Eq. (5) and 6, as well as movies of pDEP trapping of oocysts are available. See DOI: 10.1039/b000000x/

1. H. A. Pohl, *J. Appl. Phys.*, 1951, 22, 869.
2. T. B. Jones, *Electromechanics of particles*, Cambridge University Press, Cambridge ; New York, 1995.
3. R. Pethig, *Biomicrofluidics*, 2010, **4**.
4. C. F. Chou, J. O. Tegenfeldt, O. Bakajin, S. S. Chan, E. C. Cox, N. Darnton, T. Duke and R. H. Austin, *Biophys J*, 2002, **83**, 2170-2179.
5. J. Regtmeier, R. Eichhorn, M. Viefhues, L. Bogunovic and D. Anselmetti, *Electrophoresis*, 2011, **32**, 2253-2273.
6. E. B. Cummings and A. K. Singh, *Analytical chemistry*, 2003, **75**, 4724-4731.
7. S. K. Srivastava, A. Gencoglu and A. R. Minerick, *Analytical and bioanalytical chemistry*, 2011, **399**, 301-321.
8. C. F. Chou and F. Zenhausern, *IEEE engineering in medicine and biology magazine*, 2003, **22**, 62-67.
9. A. Salmanzadeh, L. Romero, H. Shafiee, R. C. Gallo-Villanueva, M. A. Stremler, S. D. Cramer and R. V. Davalos, *Lab on a chip*, 2012, **12**, 182-189.
10. N. Swami, C. F. Chou, V. Ramamurthy and V. Chaurey, *Lab on a chip*, 2009, **9**, 3212-3220.

11. W. A. Braff, A. Pignier and C. R. Buie, *Lab on a chip*, 2012, **12**, 1327-1331.
12. V. Chaurey, A. Rohani, Y. H. Su, K. T. Liao, C. F. Chou and N. S. Swami, *Electrophoresis*, 2013, **34**, 1097-1104.
13. K. T. Liao, M. Tsegaye, V. Chaurey, C. F. Chou and N. S. Swami, *Electrophoresis*, 2012, **33**, 1958-1966.
14. B. H. Lapizco-Encinas, R. V. Davalos, B. A. Simmons, E. B. Cummings and Y. Fintschenko, *J Microbiol Meth*, 2005, **62**, 317-326.
15. B. G. Hawkins, A. E. Smith, Y. A. Syed and B. J. Kirby, *Analytical chemistry*, 2007, **79**, 7291-7300.
16. A. Rohani, W. Varhue, Y. H. Su and N. S. Swami, *Electrophoresis*, 2014.
17. Y. H. Su, M. Tsegaye, W. Varhue, K. T. Liao, L. S. Abebe, J. A. Smith, R. L. Guerrant and N. S. Swami, *Analyst*, 2014, **139**, 66-73.
18. B. J. Sanghavi, W. Varhue, J. L. Chavez, C. F. Chou and N. S. Swami, *Analytical chemistry*, 2014, **86**, 4120-4125.
19. R. Pethig, A. Menachery, S. Pells and P. De Sousa, *J Biomed Biotechnol*, 2010.
20. Ting, J.W.; Peng, W. -P; Chang, H. -C, *Nuclear Science Symposium Conference Record, 2003 IEEE* , 2, 1247-1249.